J Solid State Electrochem (2015) 19:3145–3156
DOI 10.1007/s10008-015-2943-3

ORIGINAL PAPER

Structure and electrochemical properties of polystyrene/CNT nanocomposites

Miftah U. Khan[1] · **Mariam T. Darestani**[1,2] · **Vincent G. Gomes**[1]

Received: 24 December 2014 / Revised: 21 June 2015 / Accepted: 23 June 2015 / Published online: 3 July 2015

Abstract The realization of the outstanding properties of CNTs (carbon nanotubes) is constrained by their inherent tendency to agglomerate. Emulsion polymerization was used for synthesizing poly(styrene)/CNT nanocomposites with functionalized CNTs. Chain transfer agents (CTAs) were incorporated to control polymer molar mass and end-use properties. Data from electrical impedance spectroscopy (EIS) at variable frequencies were analyzed to characterize and elucidate the electrical characteristics of poly(styrene) (PS)/CNT nanocomposites. The incorporation of CNT in the polymer matrix even at modest concentrations enhanced the electrical properties of the non-conductive poly(styrene) significantly as revealed by EIS spectra. The use of CTA enabled modulation of polymer molar mass and variation in the electrical properties for PS/CNT relative to composites with no CTA. The electrical behavior of PS/CNT dispersion has been shown to depend both on the CNT concentration and molecular weight of the substrate. The equivalent electrical circuit (EEC) analyses with the corresponding system parameters enabled determination of relative CNT arrangements for different types of PS/CNT composites. TEM images confirmed the CNT positions within the composites and helped support interpretation of EIS/EEC data.

Keywords Carbon nanotube · Chain transfer agent · Polymer nanocomposite · Electrical impedance spectroscopy · Equivalent electrical circuit

✉ Vincent G. Gomes
vincent.gomes@sydney.edu.au

[1] School of Chemical and Biomolecular Engineering, The University of Sydney, Sydney, NSW 2006, Australia

[2] Science and Engineering Faculty, Queensland University of Technology, Brisbane, QLD 4000, Australia

Introduction

Carbon nanotubes (CNTs) have been receiving substantial attention because of their extraordinary mechanical, thermal, and electrical properties [1–3]. They have highly accessible surface area, low electrical resistance, high mechanical and chemical stability, and superior performance relative to other types of carbon materials in terms of reaction rates [4]. These extraordinary properties of CNTs can be harnessed efficiently when they are integrated into polymer matrices in the form of composite materials.

The enhancement of physical interaction between nanotubes and polymers namely improved dispersion of CNTs in polymer matrix can be achieved by surface modification of nanotubes. Covalent linkage between nanotubes and the polymer can lead to improved interfacial interaction [5]. Functionalization of raw CNTs can lead to formation of additional dipole-dipole interactions between CNTs and the polymeric matrix, resulting in a strengthened interface and improved dispersibility. Functionalization with even <1 wt% CNT can improve the interaction between the nanotubes and the polymer matrix [6]. Recent efforts have focused on improving the dispersion of CNT in the aqueous phase based on optimizing the physical [7] and chemical treatments [8]. Among physical methods, solution processing and melt blending have been reported [3]. Among chemical methods, in situ emulsion polymerization has been challenging because of the difficulties associated with CNT dispersion in water. Thus, the environmentally friendly, safe, and versatile technique of emulsion polymerization has received limited

attention, focusing only on improving CNT aqueous dispersion through surface modifications as a preparatory step [9]. Our goal was to obtain composites with controlled molar mass and structure via functionalization and use of chain transfer agents (CTAs) and to investigate the corresponding effects on product properties. CTAs are widely used with emulsion polymerization [10, 11]; however, few report the effect of CTA on polymer nanocomposites with the exception of Akat et al. [12] where the effect of CTA on composite synthesis and thermal property improvement with clay filler was reported. Thus, the effect of functionalized CNT with in situ emulsion polymerization and modulated molar mass on composite electrical properties is yet to be elucidated.

Electrical impedance spectroscopy (EIS) measures the dielectric properties of a medium as a function of frequency [13] and is useful in characterizing electrochemical systems. This technique measures the impedance of a system with frequency scanning to obtain broad-range frequency response to determine energy storage and dissipation characteristics. EIS has been applied to the dissolution of metals [14], corrosion inhibition [15], evaluation of corrosion rates [16], corrosion protection by polymer coatings [17], polymer electrolyte fuel cells [18], and similar applications. Vu et al. [19] reported the redox processes of polythiophene-TiO_2 nanocomposites using EIS. CNT loading to epoxy resin and its impact on EIS measurements was reported where the nanocomposites were prepared by solution mixing and subsequent hardening [4]; a rather high concentration of MWNT (20 wt%) was used in this work.

Conventional emulsion polymerization produces polymer chains with high polydispersity index (PDI) and uncontrolled molar mass [10]. Therefore, when synthesizing polymer/CNT nanocomposites, some of the CNTs are entangled by relatively long chains while others are surrounded by the short ones. Such orientations of CNT in polymer nanocomposites are favorable for creating free CNTs around or outside the polymer particle. However, when controlled chains are produced (e.g., with use of CTA), the polymer chains are expected to be uniform with shorter average lengths. Thus, the CNTs in such nanocomposites are expected to be uniformly surrounded by polymer chains of similar lengths. As a consequence, free CNTs outside the polymer particle will be restrained when low CNT concentration is used. Hence for polymer/CNT nanocomposites with CTA, CNTs are expected to be predominantly within the particle rather than at the periphery.

Coster et al. [20] reported that electrical fields travel around or outside the particle at lower frequencies but through particle internal structure at higher frequencies particularly for particles with circular profiles. Thus, enhanced electrical response is expected at lower frequencies for polymer/CNT nanocomposites with uncontrolled conventional polymerization and at higher frequencies for ones with controlled process (e.g., composites with CTA). It has been reported that mechanical properties are expected to improve with homogeneous CNT dispersion [21], while thermal degradation of composites will mainly depend on heat dissipation characteristics of CNT [22]. The absence of free CNT is likely to adversely affect thermal degradation characteristics for poly(styrene) (PS)/CNT composites when CTA is used. Jordan et al. [23] noted that for amorphous polymers, glass transition temperature increases with decreasing particle size which occurs when CTA is used in emulsion polymerization [24]. Thus, the use of CTA is expected to enable improved mechanical properties and glass transition temperature for polymer/CNT composites though the thermal degradation temperature is reduced. Electrical responses are expected to improve mostly at higher frequencies when the applied electrical field passes through the particle.

In this work, we plan to investigate the effect of variable molar mass on the electrical behavior of PS/CNT nanocomposites synthesized via in situ emulsion polymerization. These will be compared to those for pure PS. CNTs will be functionalized to establish polymerizable sites and improve aqueous dispersion to facilitate the polymerization process. EIS will be used to measure the impedance, conductance, and capacitance of pure PS and PS/CNT nanocomposites. INPHAZE™ EIS Analyzer software will be used to model the EIS measurements and determine equivalent electrical circuits (EECs) to interpret nanocomposite structures. The nanocomposites will be synthesized using modest CNT concentrations (0.3–0.7 wt%), and the effect of CTA to reduce the molecular mass of polymer will be investigated. TEM images of composites will enable investigation of CNT particle positions in synthesized nanocomposites.

Experimental setup

Functionalization of CNT

The multi-wall CNT, obtained from the Laboratory for Sustainable Technology at The University of Sydney, was prepared by the CVD technique via catalytic deposition of ethylene over Fe impregnated non-porous alumina catalyst. The CNT was purified to over 92 % purity by acid reflux method. Our dual-step approach with non-covalent and covalent functionalization [9] was used to purify and functionalize the CNT. The two-step method was designed to improve the efficiency of the covalent step where the long-chain unsaturated fatty acid (oleic acid) was used as a functionalizing agent. Functionalization improves the CNT aqueous dispersion and enables attachment of reactable functional groups on CNT side-walls. The zeta potential and FTIR measurements were used to confirm the improved aqueous phase dispersibility and the presence of reactable weak C=O bonds in the CNT structure, which were described in details earlier [9].

PS/CNT nanocomposite synthesis

In situ emulsion polymerization was conducted to synthesize poly(styrene)/carbon nanotube, i.e., PS/CNT nanocomposites. Two types of nanocomposites were prepared: PS/CNT and PS/CNT with CTA (PS/CNT_CTA) with 0.3–0.7 wt% CNT for both nanocomposites. Pure PS was synthesized from styrene (Sigma-Aldrich) after removing butylcatechol inhibitor. Functionalized CNTs were then ultrasonicated for 10 min in water before introduction into the reactor. Subsequently, measured amount of functionalized CNT, surfactant SDS (as received from Sigma-Aldrich), de-ionized water, and *n*-dodecyl mercaptan (for PS/CNT_CTA composites) from Sigma-Aldrich was poured into the 1-L reactor (PDC, USA) equipped with magnetically driven agitator and thermal transducers. Nitrogen was bubbled through the reactor contents to obtain an inert environment and prevent self-polymerization of styrene.

The reactor contents were agitated at 350 rpm, and the temperature was controlled using Julabo (Germany) heater/circulator until 70 °C was reached. Subsequently, the initiator (KPS) and buffer ($NaHCO_3$) kept at 70 °C were added into the reactor. Our typical recipe with in situ emulsion polymerization for PS/CNT (0.3 %) with CTA was styrene (monomer) 75 g, sodium dodecyl sulfate (surfactant) 1.2 g, potassium persulfate (initiator) 0.3 g, sodium bi-carbonate (buffer) 0.05 g, de-ionized water 400 g, functionalized CNT 0.225 g (for 0.3 wt%), and *n*-dodecyl mercaptan (CTA) 1 g. The reaction was allowed to continue for 3 h after which solid samples were obtained by drying the emulsion product in an oven for 24 h.

Nanocomposite characterization

Viscometry was used to obtain the molecular weights of pure PS and PS/CNT composites. The molecular weights of the samples were measured using the viscometry method. Powdered samples of PS and PS/CNT composites were dissolved in tetrahydrofuran (THF) to prepare the solution concentration of 0.5 g/dL. Thereafter, the 15-mL capillary viscometer was rinsed with THF and placed in a water bath at 25 °C. A 10-mL pipette was used to draw the THF in the capillary until it passed the calibration mark. Subsequently, the pipette bulb was released when the liquid level reached the first calibrated line. As the liquid level reached the second calibration line, the flow time was recorded. This process was repeated thrice for accuracy. The same procedure was applied for three different concentrations of each sample. The molecular weight of the samples was determined using the Mark-Houwink-Sakurada equation.

Electrochemical impedance spectroscopy (EIS) was conducted for pure PS, PS/CNT, and PS/CNT_CTA composites. In all cases, 0.5 g of the solid and dried samples synthesized via in situ emulsion polymerization were dispersed in 20-mL dispersion media, 10 mM KCl solution. The dispersions were prepared with the aid of ultrasonication. A high-resolution EIS (INPHAZE, Australia) was used with the dispersed samples at 1–10^6 Hz frequencies using gold electrodes. Measurements were repeated thrice and the average values were reported. The EIS Analyzer software was employed to model the EIS measurements which suggested corresponding EECs for different composites.

TEM images were obtained to investigate the particle location within the composites. TEM (JEM 1400, JEOL, Japan) images were acquired with an accelerating voltage till 120 kV. Dried and powdered composite samples were prepared with tenfold dilution in ethanol. The drop casting method was employed to disperse the PS/CNT composites on a holey lacey 200-mesh carbon-coated grid.

Results and discussion

Effect of CTA on nanocomposite molar mass

Table 1 shows that the use of CTA reduced the molecular weight substantially for the polymer in the nanocomposites as reported for pure polymer [25], and the inclusion of CNT itself reduced the molecular weight, since the presence of nanofillers restrains the growth of polymer chains. Thus, reductions in molar mass are observed with increasing amounts of CNT for PS/CNT nanocomposites. The molecular weight of PS/CNT (0.7 %) CTA was found to be higher than that for PS/CNT (0.5 %) CTA. This observation is in contrast with the nanocomposite molecular weight for the same CNT concentrations when CTA was not used and is possibly because of the increased crowding effects due to CNT that results in decrease in CTA efficiency for a relatively more viscous mixture.

Table 1 The effect of CTA on molecular weight of PS/CNT composites

Sample name	Molecular weight (g/mol)	Reduction in molecular weight corresponding to PS
PS	245,889	–
PS/CNT (0.3 %)	234,470	4.64 %
PS/CNT (0.5 %)	188,117	30.71 %
PS/CNT (0.7 %)	180,070	36.55 %
PS/CNT (0.3 %)_CTA	104,941	134.31 %
PS/CNT (0.5 %)_CTA	46,426	429.63 %
PS/CNT (0.7 %)_CTA	54,762	349.01 %

EIS measurements for polymer nanocomposites

Impedance

EIS was used to measure changes in impedance (z) for PS and PS/CNT composites as a function of frequency in the range of 1–10^6 Hz. For all samples, significant drop in impedance was observed up to 10^3 Hz (Fig. 1a). Incorporation of CNT in polymer matrix without CTA improved the electrical properties from pure PS via decreasing impedance for all CNT concentrations. Nevertheless, at higher frequencies, i.e., 10^3–10^6 Hz, the impedance of PS and PS/CNT nanocomposites gradually plateaus with increase in frequency (Fig. 1b).

For the entire frequency range, the impedance patterns for PS/CNT and PS/CNT_CTA nanocomposites were distinct as shown in Fig. 1a and b. Figure 1b shows that substantial improvement in electrical properties via reducing impedance in the higher frequency zone, i.e., 10^3–10^6 Hz for PS/CNT_CTA nanocomposites over pure PS which is in contrast to PS/CNT nanocomposites without CTA. Impedance behavior was demonstrated to be consistent with CNT concentration in the higher frequency range (Fig. 1b) for PS/CNT_CTA nanocomposites. However, at lower frequency zone, i.e., 1–10^3 Hz, the PS/CNT_CTA nanocomposites impedance behavior almost coincided with the base polymer (Fig. 1a) indicating insignificant improvement of electrical properties. This phenomenon can be explained by the absence of free CNT for PS/CNT_CTA nanocomposites outside the polymer particle; hence, at lower frequencies, when the electrical fields travel around or outside the particle [20], the electrical behavior was similar to a non-conductive polymer.

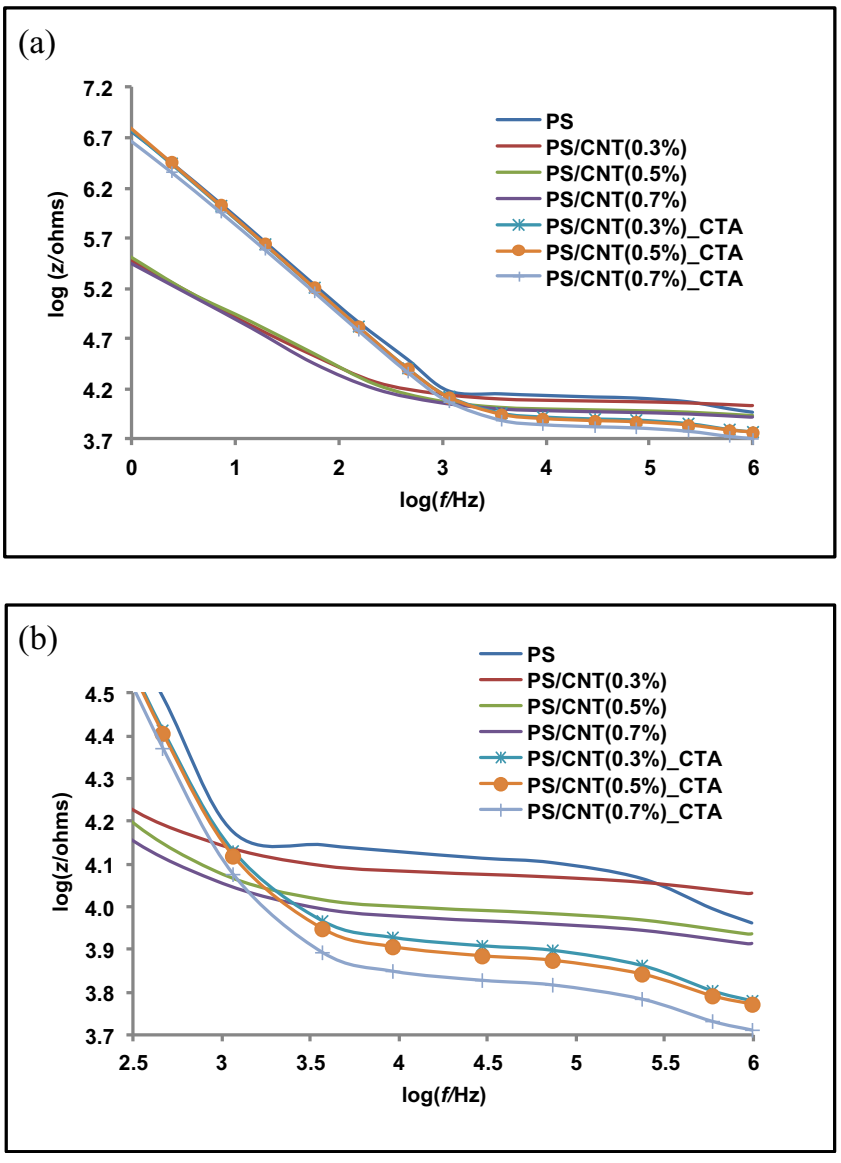

Fig. 1 Impedance of PS, PS/CNT, and PS/CNT_CTA nanocomposites for **a** frequency range 1–10^6 Hz and **b** frequency range $10^{2.5}$ to 10^6 Hz

Conductance (G)

Conductance spectra from EIS (Fig. 2a) show significantly enhanced values for PS/CNT nanocomposites relative to pure PS over the tested frequency range. Incorporation of CNT in PS matrix improves conductance even at very low frequencies ($<10^2$ Hz) for PS/CNT nanocomposites without CTA (Fig. 2b). Notably, the improvement in conductance was not consistent for CNT concentration of 0.3 and 0.5 % for lower frequency zone ($<10^2$ Hz). Though at the frequency zone $>10^{2.5}$ Hz, the conductance behavior was consistent with CNT concentration for PS/CNT nanocomposites (Fig. 2a). The results suggest that the PS/CNT nanocomposites without CTA may have free CNT as shown by enhancement of electrical conductance over pure PS particularly at the lower frequency ($<10^3$ Hz).

Figure 2a and b was able to demonstrate some notable changes in conductance for PS/CNT nanocomposites over pure PS when CTA was used in the synthesis process. The change in conductance behavior for the PS/CNT_CTA nanocomposites remained distinguishable from pure PS, and the improvement is more predominant in the higher frequency ($>10^3$ Hz) zone (Fig. 2a). At lower frequency, the conductance response for the PS/CNT_CTA nanocomposites was almost coincided with pure PS (Fig. 2b), which indicates the insignificant presence of free CNT for PS/CNT_CTA nanocomposites in comparison to the PS/CNT nanocomposites when CTA was not used in the synthesis process.

Figure 2a characterizes completely different conductance patterns for PS/CNT nanocomposites depending on the presence of CTA during the synthesis process over the large frequency range (up to 10^6 Hz). PS/CNT nanocomposites without CTA were able to demonstrate highly conductive behavior

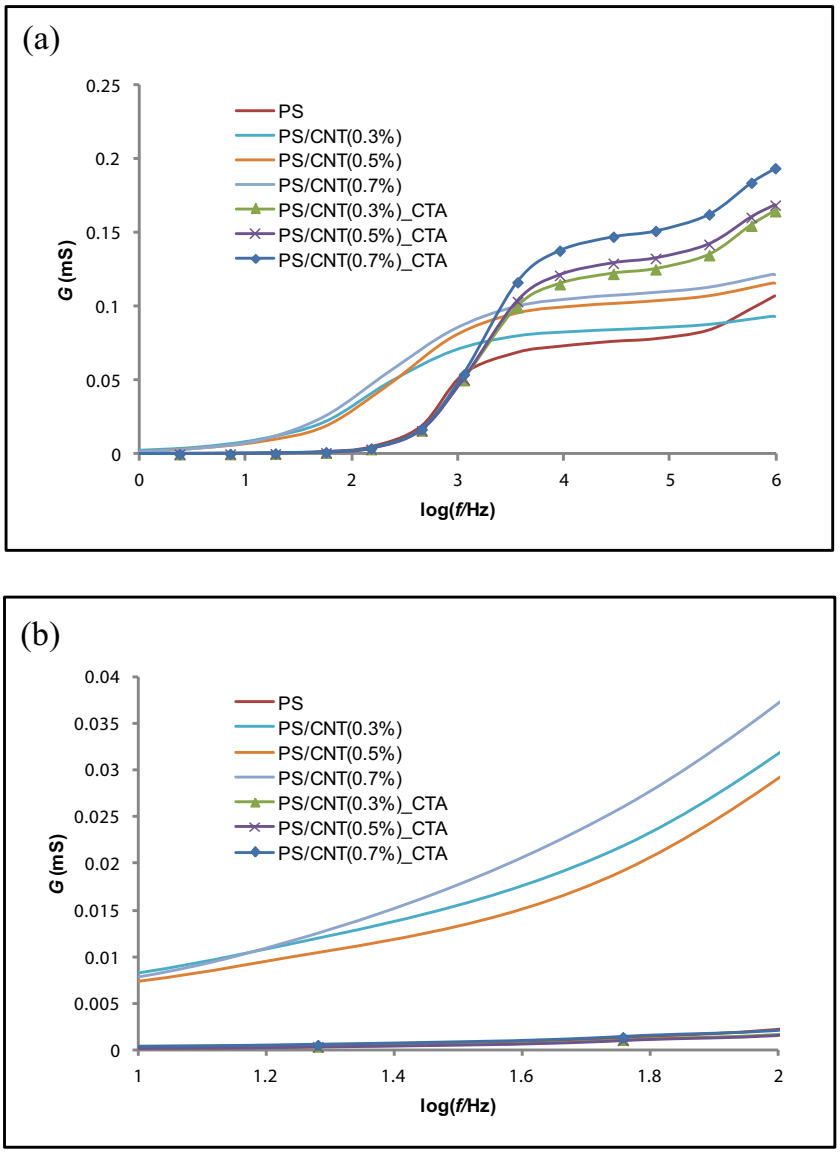

Fig. 2 Conductance of PS, PS/CNT, and PS/CNT_CTA nanocomposites for frequency range **a** 1–10^6 Hz and **b** 10–10^2 Hz

at lower frequencies; whereas, incorporation of CTA in the nanocomposites refrained them to behave such at those frequencies (Fig. 2b). Another notable observation was the shift of conductance pattern for the nanocomposites. In the frequency range 10^3–$10^{3.5}$ Hz, the conductance values for PS/CNT nanocomposites were found to get stable; whereas, the conductance values for the PS/CNT_CTA nanocomposites took over and demonstrated an enhance (Fig. 2a).

Capacitance (C)

Capacitance through a wide range of frequencies for pure PS and PS/CNT nanocomposites was measured by EIS which are shown in Fig. 3a and b.

The increased capacitance for PS/CNT nanocomposites without CTA till about $10^{2.5}$ Hz (Fig. 3a) over pure PS and PS/CNT_CTA composites suggests that the effect of CNT concentration is consistent with the substantially increased values even at low frequency (up to 10 Hz). The increment

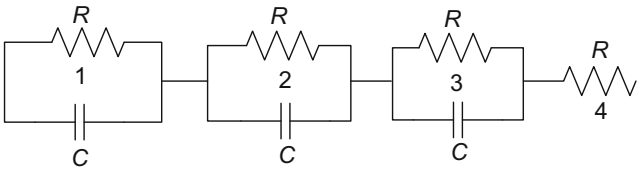

Fig. 4 Equivalent electrical circuit for PS, PS/CNT, and PS/CNT_CTA nanocomposites

in capacitance was evident even with modest CNT (0.3 %) for PS/CNT nanocomposites without CTA. However, the change in capacitance for the PS/CNT nanocomposites without CTA over pure PS at higher frequency zone (>$10^{2.5}$ Hz) was not significant irrespective of CNT concentrations (Fig. 3a).

Figure 3a shows changes in PS/CNT_CTA nanocomposite electrical behavior in terms of capacitance over pure PS. The increase in capacitance in such cases was not noteworthy in comparison to the pure PS at lower frequencies (up to around $10^{2.5}$ Hz) due to the absence of free CNT around the particle as a result of CNT entanglement with short polymer chains.

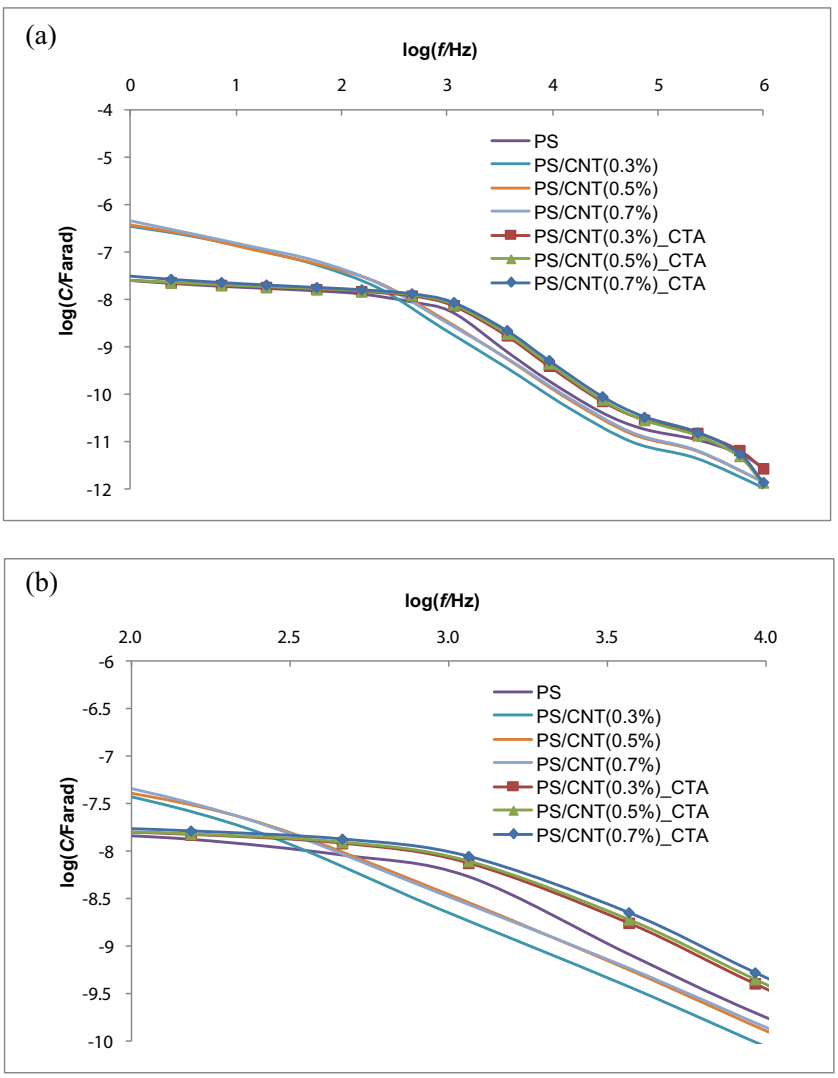

Fig. 3 Capacitance of PS, PS/CNT, and PS/CNT_CTA nanocomposites for frequency range **a** 1–10^6 Hz and **b** 10^2–10^4 Hz

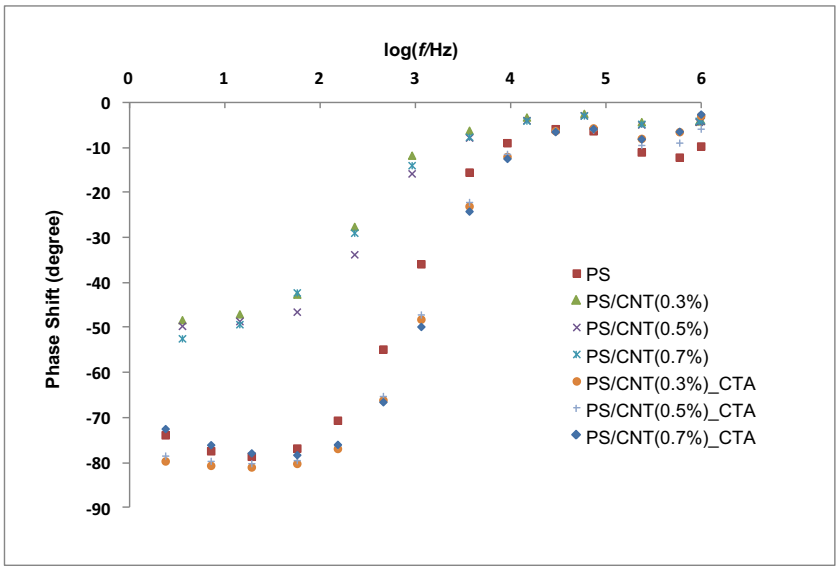

Fig. 5 Phase shift for PS, PS/CNT, and PS/CNT_CTA nanocomposites from the experimental data

However, at higher frequencies (>$10^{2.5}$ Hz), PS/CNT_CTA composites show improved capacitive behavior over pure polymer (Fig. 3b). PS/CNT and PS/CNT_CTA nanocomposites show distinct capacitance profiles, though the capacitance values decrease significantly with increased frequency throughout the measurement range for pure PS and both types of nanocomposites. This indicates that capacitance is a less dominant electrical property at higher frequencies. The capacitance values for the PS/CNT_CTA nanocomposites were almost constant up to 10^3 Hz, and thereafter, they decrease significantly (Fig. 3a) for all samples, a behavior suitable for use as sensors.

Overall, enhanced electrical behavior was obtained at lower frequencies (<10^3 Hz) for PS/CNT compared to PS/CNT_CTA nanocomposites, which were relatively insulating at those frequencies and suggest the lack of free CNT in the matrix. Mamunya et al. reported increased dielectric constant for polymer/CNT nanocomposites at low frequencies (<10^3 Hz), while at higher frequencies, the corresponding values were closer to those of the pure polymer [26]. In our work, the electrical properties showed improvement for PS/CNT_CTA nanocomposites over pure PS and PS/CNT nanocomposites without CTA at higher frequencies (>10^3 Hz). These observations indicate entanglement of CNT by similar-sized polymer chains which restrain free CNT. As a result, PS/CNT_CTA nanocomposites present superior electrical response at higher frequencies (>10^3 Hz), when the electrical field passes through the CNT inside the particle [20].

Modeling equivalent electrical circuit

The formulation of equivalent electrical circuit (EEC) is a key technique to analyze EIS data [27]. However, choosing the most appropriate equivalent circuit can be difficult because more than one set of circuits may be used to represent a particular impedance data [28]. In this study, no specific circuit was selected in advance; an electrical circuit was fitted to the EIS data for each sample and optimized using the INPHAZE™ EIS Analyzer software based on a nonlinear least-square-error method [29]. Results for pure PS, PS/CNT, and PS/CNT_CTA nanocomposites were analyzed to cover all samples we synthesized. The EEC model comprises four elements in series: elements 1, 2, and 3 are Maxwell-Wagner elements with a capacitance (C) and a resistance (R) in parallel, while element 4 is a resistance. Time

Table 2 Frequency constants of EEC elements for PS, PS/CNT, and PS/CNT_CTA nanocomposites

Sample	Frequency constant: element 1 (Hz)	Frequency constant: element 2 (Hz)	Frequency constant: element 3 (Hz) ($\times 10^2$)	Frequency constant: element 4 (Hz) ($\times 10^5$)
PS	0.23	4.03	1.06	7.16
PS/CNT (0.3 %)	0.62	24.18	5.95	9.44
PS/CNT (0.5 %)	0.65	34.42	10.95	13.26
PS/CNT (0.7 %)	0.68	25.97	9.39	12.54
PS/CNT (0.3 %)_CTA	0.15	2.19	0.55	5.41
PS/CNT (0.5 %)_CTA	0.09	2.25	0.49	7.42
PS/CNT (0.7 %)_CTA	0.19	2.27	0.42	7.25

Table 3 Time constants (τ) of EEC elements for PS, PS/CNT, and PS/CNT_CTA nanocomposites

Sample	Time constant (τ) for element 1 (s)	Time constant (τ) for element 2 (s) ($\times10^{-2}$)	Time constant (τ) for element 3 (s) ($\times10^{-3}$)	Time constant (τ) for element 4 (s) ($\times10^{-7}$)
PS	0.69	3.95	1.50	2.2
PS/CNT (0.3 %)	0.26	0.65	0.26	1.7
PS/CNT (0.5 %)	0.25	0.46	0.15	1.2
PS/CNT (0.7 %)	0.24	0.61	0.17	1.3
PS/CNT (0.3 %)_CTA	1.04	7.28	2.87	2.9
PS/CNT (0.5 %)_CTA	1.82	7.06	3.23	2.1
PS/CNT (0.7 %)_CTA	0.82	7.01	3.72	2.2

constants and frequency constants were estimated from the developed models for the EEC components shown in Fig. 4.

When a phase shift value is close to −90° and is typically at its minimum, a capacitive behavior is dominant, and when the value is almost 0°, a resistive behavior is dominant [30, 31]. Figure 5 shows phase shifts at the corresponding frequency constants (Table 2) derived from the model. The phase shifts for elements 1, 2, and 3 for PS and PS/CNT_CTA nanocomposites (close to −90°) are notably distinct from those for PS/CNT nanocomposites without CTA. Thus, for pure PS and PS/CNT_CTA nanocomposites, a dominant capacitive and less significant resistive behavior is expected for elements 1, 2, and 3.

Phase shifts for the corresponding frequency constants of elements 1, 2, and 3 for PS/CNT nanocomposites without CTA are not in the vicinity of −90° (Fig. 5), indicating the dominance of resistive (R) components in this case. However, phase shifts at the corresponding frequency constants of element 4 for all samples showed a value of almost 0°. Thus, the capacitive components (C) of the corresponding EEC can be ignored for element 4, for which the resistive (R) component suffices.

Correlating EEC with nanocomposite internal structure

Time constants (τ) of the different elements in the EEC were analyzed to elucidate the internal structure of the nanocomposites, particularly with respect to the conductive element, CNT. The time constant of an element in the EEC is $\tau=RC$, where R is resistance and C is capacitance, and $f=1/2\pi\tau$, where f is the frequency constant for the corresponding time constant.

From Tables 2 and 3, we note that the EIS model indicates decrease in time constant (τ) for EEC elements with increasing frequencies as evident from the corresponding parameters of the EEC elements. For particles of circular shape, these observations relate to the direction of electrical field applied. Higher time constants result from the electrical field traveling outside the particle which occurs at lower frequencies for all samples. In contrast, higher frequencies result in lower time constants which indicate that the applied electrical fields are responsive to the internal structure of the sample as reported by others [20].

The modeled conductance and capacitance values for the EEC elements of all samples are given in Tables 4 and 5. These enable interpreting the electrical behavior of the nanocomposites which incorporate contributions from the conductive CNT and non-conductive base polymer PS. The less dominant resistive behavior of elements 1, 2, and 3 for PS and PS/CNT_CTA nanocomposites which show negligible conductance values (Table 4) for these elements compared to PS/CNT nanocomposites without CTA is in agreement with our experimental data. On the contrary, the capacitance values for PS and PS/CNT_CTA nanocomposites for elements 1, 2, and 3 are significant compared to PS/CNT nanocomposites

Table 4 Conductance of EEC elements for PS, PS/CNT, and PS/CNT_CTA nanocomposites

Sample	Conductance for element 1 (S) ($\times10^{-7}$)	Conductance for element 2 (S) ($\times10^{-6}$)	Conductance for element 3 (S) ($\times10^{-5}$)	Conductance for element 4 (S) ($\times10^{-5}$)
PS	0.4	1.33	3.13	7.74
PS/CNT (0.3 %)	8.9	11.7	5.5	8.90
PS/CNT (0.5 %)	17.4	22.0	7.99	10.17
PS/CNT (0.7 %)	17.1	26.6	8.54	10.63
PS/CNT (0.3 %)_CTA	0.1	1.60	2.10	10.20
PS/CNT (0.5 %)_CTA	0.2	1.25	1.64	12.77
PS/CNT (0.7 %)_CTA	0.5	0.97	1.28	14.58

Table 5 Capacitance of EEC elements for PS, PS/CNT, and PS/CNT_CTA nanocomposites

Sample	Capacitance for element 1 (F) ($\times 10^{-8}$)	Capacitance for element 2 (F) ($\times 10^{-8}$)	Capacitance for element 3 (F) ($\times 10^{-8}$)	Capacitance for element 4 (F) ($\times 10^{-11}$)
PS	2.92	5.24	4.68	2.0
PS/CNT (0.3 %)	22.90	7.70	4.60	1.0
PS/CNT (0.5 %)	42.93	10.17	4.55	1.0
PS/CNT (0.7 %)	39.97	16.30	4.56	1.0
PS/CNT (0.3 %)_CTA	1.04	11.65	6.03	3.0
PS/CNT (0.5 %)_CTA	2.73	8.82	5.28	3.0
PS/CNT (0.7 %)_CTA	3.94	6.80	4.74	3.0

(Table 5). These observations confirm that elements 1, 2, and 3 have comparatively dominant capacitive behavior for PS and PS/CNT_CTA nanocomposites. Negligible capacitance values for element 4 along with significant conductance for the same element for all nanocomposites justify accepting a solely resistive component for element 4 (Fig. 4).

Higher time constants at lower frequencies for elements 1, 2, and 3 suggest that the electrical fields travel outside the particle [20]. At the same time, the lower conductance of PS/CNT_CTA nanocomposites for these elements indicates the absence of free CNT around the polymer particle. This observation from the modeled data supports the phenomena of adequate coverage of CNT by PS due to the uniformly sized polymer chains when CTA is used for nanocomposite synthesis. This coverage by polymer molecules renders the PS/CNT_CTA nanocomposites predominantly polymer-like in terms of electrical behavior at low frequencies. This is in agreement with our EIS measurements for electrical properties. The significant conductance of PS/CNT nanocomposites without CTA for elements 1, 2, and 3 at low frequencies signifies the presence of free CNT around the particles due to the random arrangement of CNT and non-uniform polymer chain length.

Element 4 for all nanocomposites at higher frequencies is represented by a resistive component only (Fig. 4). The low time constant (τ) of this element for all nanocomposites (Table 3) indicates that the directional vector of the applied electrical field is through the particle. Figure 6 shows that the conductance of EEC element 4 for PS/CNT and PS/CNT_CTA increases with CNT content with a steeper slope for PS/CNT_CTA, suggesting that the conductive component (CNT) is inside the particle for the latter.

PS/CNT_CTA nanocomposites showed higher conductance at higher frequency, suggesting that the CNT particles are predominantly coated by polymer chains. On the other hand, the lower conductance of PS/CNT nanocomposites without CTA for element 4 suggests the presence of free CNT primarily outside the polymer particle. The EEC results suggest that a fraction of the CNT remain free, and the rest are entangled by polymer chains for PS/CNT nanocomposites without CTA, while for PS/CNT_CTA nanocomposites, CNTs are primarily entangled by polymer chains.

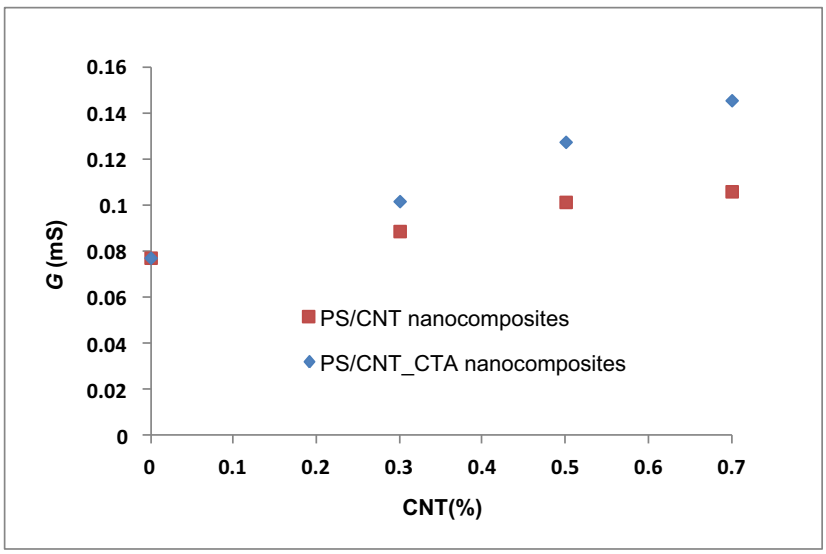

Fig. 6 Conductance of EEC element 4 for PS/CNT and PS/CNT_CTA nanocomposites

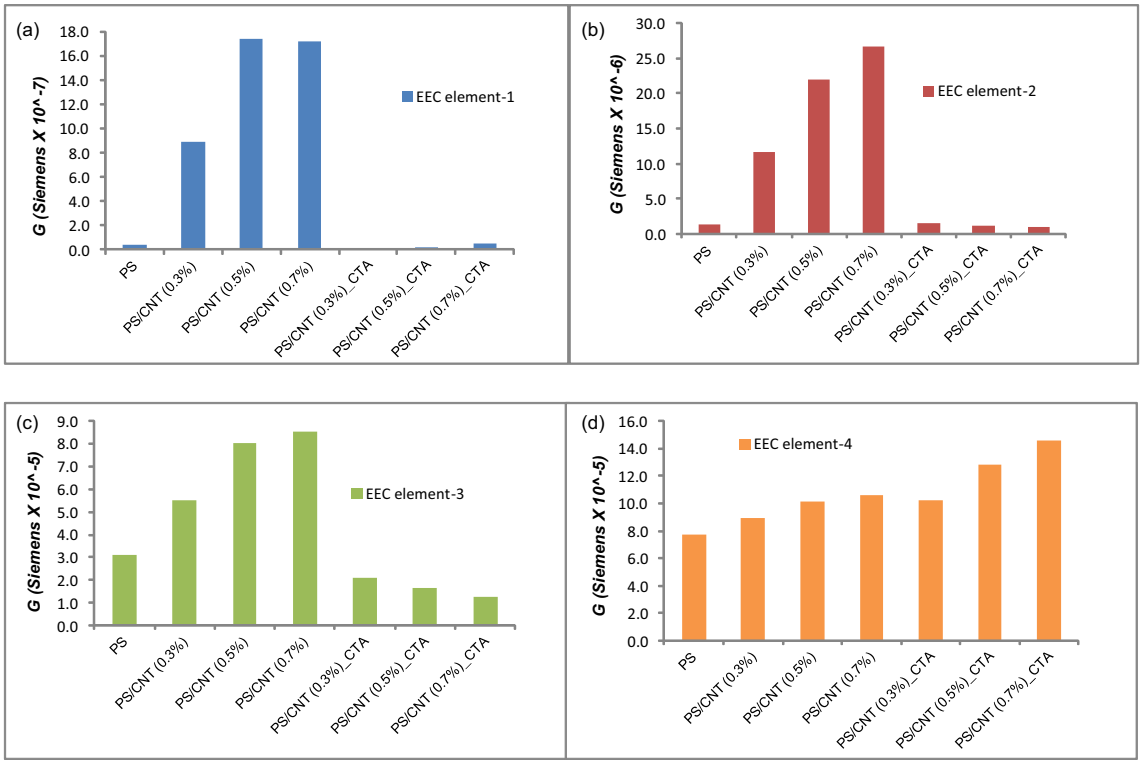

Fig. 7 **a**, **b**, **c**, **d** Conductance of frequency dependent EEC elements: elements 1, 2, and 3 (<10^3 Hz) and element 4 (~10^6 Hz)

Comparison of conductance behavior for EEC elements

The frequency dependent conductance properties of the EEC elements for the different samples are shown in Fig. 7.

Figure 7 represents the conductance behavior for the EEC elements derived from the model. At low frequencies (<10^3 Hz; Fig. 7a–c), the PS/CNT nanocomposites without CTA showed distinctively superior conductive behavior over pure PS and PS/CNT_CTA nanocomposites. This observation is in agreement with EIS measurements presented in Fig. 2a and b, which show that the conductance for PS/CNT_CTA nanocomposites is insignificant in comparison with PS/CNT nanocomposites for EEC elements 1 and 2. However, for EEC element 3, the conductance of PS/CNT_CTA starts to show significance and indicates a prelude to shifts at higher frequencies and is consistent with the EIS measurements shown in Fig. 2a. At higher frequency (10^6 Hz, Fig. 2a), EIS data are consistent with the EEC parameters on conductance for element 4 (Fig. 7d). In both cases, at a frequency of around 10^6 Hz, the PS/CNT_CTA nanocomposites show enhanced conductance over that of the PS/CNT nanocomposites without CTA for similar CNT concentrations. Moreover, the consistent increment in conductance with increased CNT concentration at higher frequencies for both types of nanocomposites shown via EIS measurements (Fig. 2a) is reflected in the conductance for EEC element 4 (Fig. 7d). These observations suggest that the modeled EEC elements reasonably represent the electrical behavior of the samples tested.

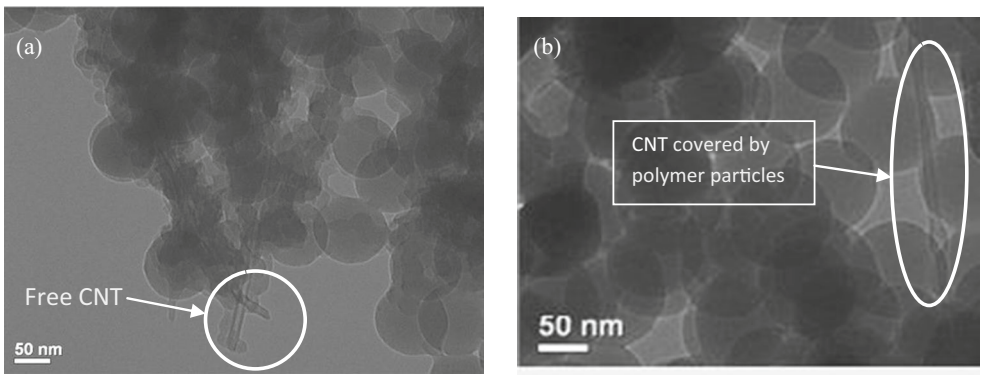

Fig. 8 TEM images for PS/CNT (0.5 wt%) nanocomposites **a** without CTA and **b** with CTA

TEM images of polymer nanocomposites

To compare particle position and investigate the presence of free CNTs which affect the electrical property at low frequencies, we analyzed the TEM images of PS/CNT nanocomposites without CTA (Fig. 8a) and with CTA (Fig. 8b).

Figure 8a shows the presence of free CNT for PS/CNT nanocomposites without CTA; however, these were not observed for PS/CNT_CTA nanocomposites (Fig. 7b). However, with CTA, the CNT was found to be covered reasonably uniformly by polymer particles having circular profiles for PS/CNT_CTA nanocomposites (Fig. 8b). Thus, the TEM observations are in agreement with the electrical measurements for the nanocomposites in terms of their frequency-dependent electrical characteristics. The TEM images show that the polymer particles for both nanocomposites mostly have circular profiles as expected for spherical shaped particles; this satisfies our explanations for time constants (τ) with reference to composite structure and transit direction for the applied electrical field.

Conclusions

PS/CNT nanocomposites having variable CNT contents and molecular weights were synthesized and investigated for their electrical properties using the EIS. Both the CNT and CTA contents were found to have profound influence on the nanocomposites; in particular, the electrical behavior was characterized using the EIS and equivalent electrical circuits and the CNT locations via TEM images. The nanocomposites were synthesized via in situ emulsion polymerization with functionalized CNT to improve the aqueous dispersibility and to impart polymerizable sites. The electrical properties of PS/CNT nanocomposites were enhanced significantly at modest levels of CNT concentrations. CTA incorporation was found to affect not only the molecular weight but also the electrical properties of the nanocomposites remarkably at low frequencies compared with PS/CNT nanocomposites without CTA. The electrical behavior was due to the traversing direction of the applied electrical field at low frequencies being outside the polymer particles. In contrast, EIS was able to detect a shift in electrical behavior towards PS/CNT_CTA nanocomposites at higher frequencies when the applied electrical field is expected to travel through the particle. The shifts in behavior were mostly in the frequency range of 10^3 Hz. EECs derived from EIS modeling in conjunction with time constant data were used to explain the observed electrical behavior and relate them to CNT position in the nanocomposites. The capacitive responses of PS/CNT_CTA nanocomposites suggest their potential for application in sensors. EIS modeling for the nanocomposites was used to derive the equivalent electrical circuits (EECs) and their corresponding parameters, which were found to be distinct based on whether CTA was used in the synthesis process. The acquired TEM images support the effect of CNT arrangement within the nanocomposites as shown from EEC analyses.

Acknowledgments The authors acknowledge the support from the Australian Research Council and fruitful discussions with Prof. Hans Coster.

References

1. Dumitrescu L, Wilson NR, Macpherson JV (2007) Functionalizing single-walled carbon nanotube networks: effect on electrical and electrochemical properties. J Phys Chem 111:12944–12953
2. Katz E, Willner I (2004) Biomolecule-functionalized carbon nanotubes: applications in nanobioelectronics. ChemPhysChem 5: 1084–1104
3. Moniruzzaman M, Winey KI (2006) Polymer nanocomposites containing carbon nanotubes. Macromolecules 39:5194–5205
4. Olivé-Monllau R, Esplandiu MJ, Bartrolí J, Baeza M, Céspedes F (2010) Strategies for the optimization of carbon nanotube/polymer ratio in composite materials: applications as voltammetric sensors. Sensors Actuators B 146:353–360
5. Philip B, Abraham JK, Chandrasekhar A, Varadan VK (2003) Carbon nanotube/PMMA composite thin films for gas-sensing applications. Smart Mater Struct 12:935–939
6. Frankland SJV, Caglar A, Brenner DW, Griebel M (2002) Molecular simulation of the influence of chemical cross-link on the shear strength of CNT-polymer interface. J Phys Chem 106: 3046–3048
7. Yu J, Grossiord N, Koning CE, Loos J (2007) Controlling the dispersion of multi-wall carbon nanotubes in aqueous surfactant solution. Carbon 45:618–623
8. Wang Y, Iqbal Z, Mitra S (2005) Rapidly functionalized, water-dispersed carbon nanotubes at high concentration. J Am Chem Soc 128:95–99
9. Khan MU, Gomes VG, Altarawneh IS (2010) Synthesizing polystyrene/carbon nanotube nanocomposites by emulsion polymerization with non-covalent and covalent functionalization. Carbon 48:2925–2933
10. Altarawneh I, Gomes VG, Srour M (2009) Polymer chain extension in semibatch emulsion polymerization with RAFT-based transfer agent: the influence of reaction conditions on polymerization rate and product properties. J Appl Polym Sci 114(4):2356–2372
11. O'Donnell KJ, Eric W (2010) Reversible addition–fragmentation chain transfer in microemulsions: effect of chain transfer agent aqueous solubility. Macromolecules 43(4):1730–1738
12. Akat H, Atilla MT, Filip DP, Yusuf Y (2008) Synthesis and characterization of polymer/clay nanocomposites by intercalated chain transfer agent. Eur Polym J 44:1949–1954
13. Volkov AA, Prokhorov AS (2003) Broadband dielectric spectroscopy of solids. Radiophys Quantum Electron 46:657–665
14. Cai M, Park SM (1996) Oxidation of zinc in alkaline solutions studied by electrochemical impedance spectroscopy. J Electrochem Soc 143:3895–902
15. Sherif EM, Park SM (2006) Effects of 1,4-naphthoquinone on aluminum corrosion in 0.50 M sodium chloride solutions. Electrochima Acta 51:1313–21
16. Scully JR (2000) Polarization resistance method for determination of instantaneous corrosion rates. Corrosion 56:199–218

17. Mansfeld F (1995) Use of electrochemical impedance spectroscopy for the study of corrosion protection by polymer coatings. J Appl Electrochem 25:187–202
18. Danzer MA, Hofer EP (2009) Analysis of the electrochemical behaviour of polymer electrolyte fuel cells using simple impedance models. J Power Sources 190:25–33
19. Vu QT, Pavlik M, Hebestreit N, Rammelt U, Plieth W, Pfleger J (2005) Nanocomposites based on titanium dioxide and polythiophene: structure and properties. React Funct Polym 65: 69–77
20. Coster HGL, Chilcott TC, Coster ACF (1996) Impedance spectroscopy of interfaces, membranes and ultrastructures. Bioelectroch Bioener 40:79–98
21. Gojny FH, Wichmann MHG, Köpke U, Fiedler B, Schulte K (2004) Carbon nanotube-reinforced epoxy-composites—enhanced stiffness and fracture toughness at low nanotube contents. Compos Sci Technol 64:2363–71
22. Song PC, Liu CH, Fan SS (2006) Improving the thermal conductivity of nanocomposites by increasing the length efficiency of loading carbon nanotubes. Appl Phys Lett 88:153111-(1–3)
23. Jordan J, Jacob KI, Tannenbaum R, Sharaf MA, Jasiuk I (2005) Experimental trends in polymer nanocomposites—a review. Mater Sci Eng A 393:1–11
24. Benyahia B, Latifi MA, Fonteix C, Pla F, Nacef S (2010) Emulsion copolymerization of styrene and butyl acrylate in the presence of a chain transfer agent. Part 1: modelling and experimentation of batch and fedbatch processes. Chem Eng Sci 65:850–869
25. Gomes VG, Tjiam C (2014) Optimal operating strategies for emulsion polymerization with chain transfer agent. Ind Eng Chem Res 53:7526–7537
26. Mamunya Y (2011) Carbon nanotubes as conductive filler in segregated polymer composites—electrical properties. In Yellampalli S (ed) Carbon Nanotubes - Polymer Nanocomposites, Publisher: InTech. doi:10.5772/18878
27. Abouzari MRS, Berkemeier F, Schmitz G, Wilmer D (2009) On the physical interpretation of constant phase elements. Solid State Ionics 180:922–927
28. West AR, Sinclair DC, Hirose N (1997) Characterization of electrical materials, especially ferroelectrics, by impedance spectroscopy. J Electroceram 1:65–71
29. Chilcott TC, Wong ELS, Coster H, James M (2009) Ionic double layer of atomically flat gold formed on mica templates. Electrochim Acta 54:3766–3774
30. Abdollahi Z, Ghasemi S, Darestani M, Gomes VG (2014) Characterizing colloidal behavior of non-ionic emulsifiers in non-polar solvents using electrical impedance spectroscopy. Colloid Polym Sci 292:2695–2705
31. Ghasemi S, Abdollahi Z, Darestani M, Gomes VG (2015) Online monitoring of emulsion polymerization using electrical impedance spectroscopy. Polym Int 64:66–75